000 3834

DOT/FAA/PS-87/4

Program Engineering
Service
Washington, D.C. 20591

Development and Testing of The Gust Front Algorithm

Arthur Witt
Steven D. Smith

National Severe Storms Laboratory
1313 Halley Circle
Norman, OK 73069

November 1987

Interim Report

This document is available to the public
through the National Technical Information
Service, Springfield, Virginia 22161

U.S. Department of Transportation
Federal Aviation Administration

NOTICE

This document is disseminated under the sponsorship of the Department of Transportation in the interest of information exchange. The United States Government assumes no liability for its contents or use thereof.

Technical Report Documentation Page

1. Report No. DOT/FAA/PS-87/4	2. Government Accession No.	3. Recipient's Catalog No.
4. Title and Subtitle Development and Testing of the Gust Front Algorithm		5. Report Date November 1987
		6. Performing Organization Code MGG000
7. Author(s) Arthur Witt and Steven D. Smith		8. Performing Organization Report No.
9. Performing Organization Name and Address National Severe Storms Laboratory 1313 Halley Circle Norman, OK 73069		10. Work Unit No. (TRAIS)
		11. Contract or Grant No. DTFA01-80-Y-10524
12. Sponsoring Agency Name and Address U.S. Department of Transportation Federal Aviation Administration Program Engineering Service Washington, D.C. 20591		13. Type of Report and Period Covered Interim Report
		14. Sponsoring Agency Code APS-310

15. Supplementary Notes

16. Abstract

Threshold changes, additions, and other refinements to the original version of the Gust Front Algorithm are documented. Threshold changes include a minimum velocity difference threshold, the maximum azimuthal separation between vectors, and maximum range separation. Additions include gust front tracking and forecasting in Cartesian coordinates, vertical continuity checks of gust front features to reduce the occurrence of false detections, and horizontal wind estimation both ahead and behind a detected gust front using single Doppler velocity data. Results of these additions and the effects of threshold changes on detection capability are presented for several case studies.

17. Key Words wind shear; Doppler radar, gust fronts	18. Distribution Statement This document is available to the public through the National Technical Information Service, Springfield, Virginia 22161.

19. Security Classif. (of this report)	20. Security Classif. (of this page)	21. No. of Pages	22. Price
UNCLASSIFIED	UNCLASSIFIED	38	

Form DOT F 1700.7 (8-72) Reproduction of completed page authorized

PREFACE

We would like to thank Drs. Dusan Zrnic' and Robert Maddox, Patrick Sanford, and Ken Wilk for valuable discussions and suggestions concerning this study. Doppler radar data from Memphis and Denver was provided by MIT/Lincoln Laboratory and the National Center for Atmospheric Research, respectively. Joan Kimpel provided graphics support and Carole Holder typed the manuscript. Part of this work was supported by the Joint Systems Program Office of NEXRAD.

TABLE OF CONTENTS

Abstract

List of Figures

List of Tables

1. Introduction 1

2. New Thresholds 1

3. Significant Additions 3

3.a Curve Fitting in Cartesian Coordinates 3

3.b Vertical Continuity 4

3.c Estimates of the Wind Velocity Ahead and Behind the Gust Front 6

4. Preliminary Results 9

4.a Test Results for the Gust Front Algorithm 9

4.b Test Results for the Sectorized Uniform Wind Algorithm ... 13

4.c Comparison of SUW Estimates With the Propagation Speed of the Gust Front 21

4.d General Comments on the SUW Algorithm 23

5. Verification of Gust Front Algorithm Output 24

5.a Comparison of Gust Front Position with Surface Stations .. 24

5.b Comparison with Second Doppler Radar 28

6. Summary 29

References

LIST OF FIGURES

Figure 1. Geometry of curve fitting in cartesian coordinates. C is the center of the gust front feature.

Figure 2. Geometry of the vertical continuity box. Initially determined size is dashed and the solid line box is its final location.

Figure 3. Schematic showing detected gust front and the two data windows over which we estimate the horizontal wind. The adjustable parameters Δr, $\Delta\theta$, and δr are identified.

Figure 4. Illustrations of possible gust front orientations and the data windows over which we estimate the horizontal wind.

Figure 5. Algorithm output for the Memphis gust front of May 28, 1985 at 1615 CST. Range marks are at 30 km intervals.

Figure 6. Algorithm output for the Denver gust front of July 25, 1984 at 1702 MST for peak shear and min Δv thresholds of a) 4 m s^{-1} km^{-1} and 10 m s^{-1}, and b) 2 m s^{-1} km^{-1} and 5 m s^{-1}. Range marks are at 30 km intervals. An "F" indicates a false feature.

Figure 7. Same as Figure 6, except for the Oklahoma gust front of April 26, 1984 at 2037 CST.

Figure 8. April 13, 1981 Oklahoma gust front case showing detected position at a) 2111 CST and b) 2123 CST. SUW estimates are denoted by arrows with arrow length proportional to wind speed and arrow orientation indicating wind direction. Mesonetwork wind data are plotted as barbs with flags next to their numerical values. Long flags indicate 10 m s^{-1}, short flags indicate 5 m s^{-1}. The 2120 CST TTS rawinsonde winds up to 1 km AGL are shown in (b). The rawinsonde launch site is indicated with a balloon. The line labeled AA' describes the location of the horizontal cross-section shown in Figure 9.

Figure 9. Horizontal cross-section along line AA' shown in Figure 8b. Reflectivity factor Z (dBZ), radial velocity (m s^{-1}), and a nine-point average mean velocity are given. "B" and "E" denote the beginning and ending range of the pattern vector. "G" is the detected position of the gust front. The location and length, in range, of each data window is shown.

Figure 10. May 9, 1981 Oklahoma gust front case showing detected position at a) 0018 CST and b) 0032 CST. Symbols are as defined in Figure 8.

Figure 11. April 26, 1984 Oklahoma gust front case showing detected position at a) 2042 CST and b) 2052 CST. Symbols are as defined in Figure 8. The 1957 CST CHK rawinsonde winds up to 1 km AGL are shown in (b).

Figure 12. Plot of the algorithm output for the Oklahoma gust front of May 9, 1981 along with the locations (1,2,3) of the NSSL surface stations used for a time of passage comparison.

Figure 13. Same as Figure 12, except for April 26, 1984.

Figure 14. Same as Figure 12, except for April 13, 1981.

Figure 15. Algorithm output for two different radars; a) Norman (NRO) and b) Cimarron (CIM), looking at the same gust front (April 13, 1981).

LIST OF TABLES

Table 1. List of Thresholds

Table 2. Tower Data at 2042 and 2100 CST for the April 26, 1984 Gust Front Case

Table 3. Gust Front Propagation Speeds Obtained From Two Consecutive (In Time) Centroid Positions Along With SJW Estimates of the Wind Behind the Gust Front for the Earlier of the Two Times

Table 4. Results of the Gust Front Position Comparison for the Norman and Cimarron Radars

Development and Testing of the Gust Front Algorithm

Arthur Witt and Steven D. Smith
NOAA, Environmental Research Laboratories
National Severe Storms Laboratory
Norman, Oklahoma 73069

March 1987

1. INTRODUCTION

The initial design and development of the gust front algorithm was done by Uyeda and Zrnic' (1985, 1986). Through limited testing on several cases, they showed that the algorithm could accurately detect and track strong gust fronts that commonly occur in Oklahoma during the Spring. However, further developmental work and testing was necessary to bring the algorithm from its semi-automatic research stage to a routinely functioning, fully automated algorithm ready for operational use. The purpose of this report is to document changes and additions that have been implemented thus far, and to present initial test results for the latest version of the algorithm. Additional refinements will undoubtedly occur after real-time testing in Denver and Norman in 1987, and these results will be reported at a later date. Readers not familiar with the algorithm are advised to first read the report by Uyeda and Zrnic'(1985).

2. NEW THRESHOLDS

The most important changes to the previous thresholds affected those used to determine whether or not to save a pattern vector. A gust front pattern vector is a multi-dimensional vector that quantifies radial convergence (a sequence of decreasing velocities) and has the following attributes: azimuth, beginning range r_b, ending range r_e, beginning velocity v_b, ending velocity v_e, peak shear, and location of the peak shear. Testing by Uyeda and Zrnic' (1985) indicated that the best parameter to use for determining the strength and position of a gust front was the maximum velocity gradient, or peak shear, within a pattern vector. It was therefore decided to use the peak shear (Eq. 1 in Uyeda and Zrnic', 1985) as the primary means of determining whether or not to save a pattern vector, in place of the previous high and low grad-

ient and "flux" thresholds. To eliminate those vectors having a high peak shear, but low radial convergence (i.e., a small velocity difference), a minimum velocity difference threshold (min Δv) has been added, with the velocity difference given by $\Delta v = v_b - v_e$. The peak shear and min Δv thresholds have initially been set at 4 m s^{-1} km^{-1} and 10 m s^{-1}, respectively, which should allow for the detection of moderate to strong gust fronts based on tests with Oklahoma data. If it is also desired to detect weak gust fronts, these thresholds will likely need to be reduced, noting however, that as the thresholds are reduced, the false alarm rate will likely increase.

The criteria for grouping pattern vectors into possible gust front features have also been changed. Initial tests with the old thresholds resulted in some major grouping problems. Therefore, the threshold values were reduced by about one-half. The maximum azimuthal separation between vectors is now 2.2°, so that a gap of no more than one radial is allowed if consecutive radials are separated by 1°. The maximum range separation between consecutive vectors is now 2.0 km, with the range of a vector being given by the location of the peak shear.

In place of a height threshold, it was decided to process only two low-level scans below an elevation angle of 1.5° out to a range of 60 km. Test results using up to four elevation scans at close ranges resulted in a large increase in the false alarm rate for some cases, with no significant improvement in the detection capability. The decision to process data to distances of 60 km was made to provide at least a 20 min advanced warning of gust front passage over any airport close to the radar site.

Because it is distinctly possible that a feature with a large number of vectors could in fact cover only a small distance if it is located very close to the radar, a minimum length threshold was added. Initially, a feature must have a minimum of five vectors to be saved. Then, after the length of a feature is calculated, if its length is less than 5 km, it is discarded.

A list of the new threshold values is given in Table 1.

TABLE 1. List of Thresholds.

Threshold	Numerical Value
Peak shear	4 m s^{-1} km^{-1}
Minimum velocity difference	10 m s^{-1}
Minimum length	5 km
Minimum number of vectors in a feature	5
Maximum azimuthal separation between vectors	2.2°
Maximum range separation between vectors	2 km
Minimum reflectivity	-15 dBZ

3. SIGNIFICANT ADDITIONS

a. Curve Fitting in Cartesian Coordinates

Previously, the location of a gust front was approximated by fitting a second-order polynomial $r(\theta)$ to the individual vector locations of the peak shears (see Eq. 17 in Uyeda and Zrnic', 1985). Tracking and forecasting were performed by translating the fitted position according to the latest estimate of propagation speed. While this procedure performed well in tracking gust fronts some distance away from the radar, it may not be suitable for fronts that are close to the radar site. This is because the second-order polynomial in θ approximates well the gust fronts' parabolic shape only at appreciable distances from the radar. Therefore, it was decided to perform curve fitting and tracking in cartesian coordinates, so proximity to the radar would cause no problems.

The procedure by which curve fitting is done is shown in Figure 1. First, a local coordinate system (x', y') is established with its origin at the center of a feature. Next, a line is formed by connecting the two end points of the feature, E_1 and E_2. The local coordinate system is then rotated until the x' axis is parallel to line E_1E_2. This establishes a second local coordinate system (x", y"). The vector locations of the gust front feature are then converted from the original coordinate system to the (x", y") system, and a least-squares fit of the second-order polynomial

$$y'' = b_0 + b_1 x'' + b_2 (x'')^2 \tag{1}$$

is performed. It is this fitted curve which is used for plotting and tracking.

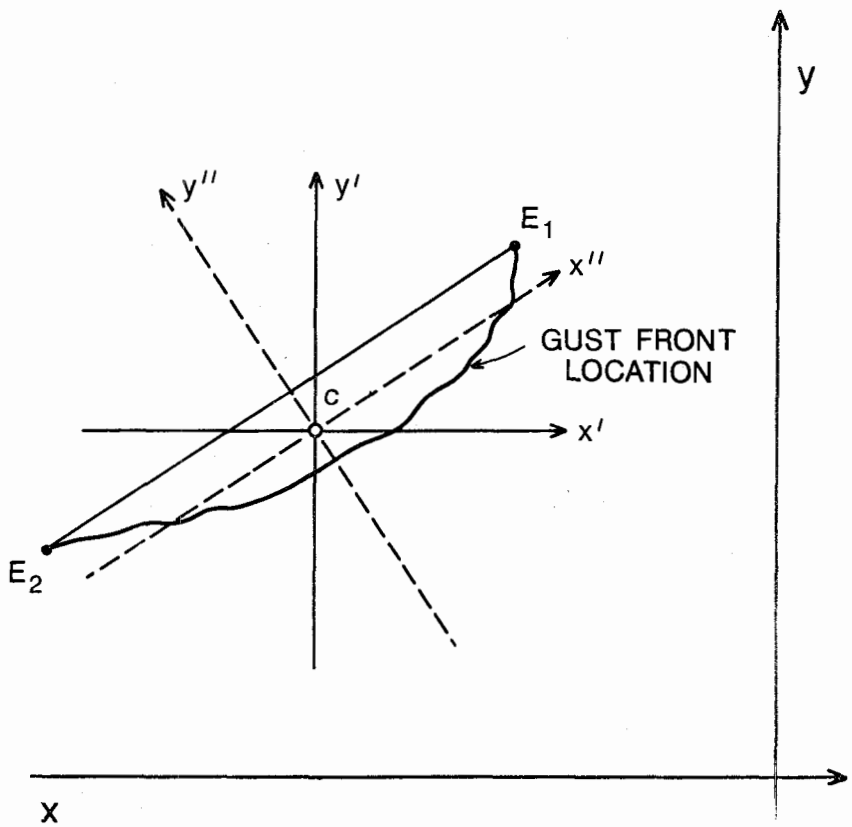

Figure 1. Geometry of curve fitting in cartesian coordinates. C is the center of the gust front feature.

b. Vertical Continuity

The initial version of the algorithm operated on only one elevation scan of radar data. This, unfortunately, resulted in a very high false alarm rate. Consequently, the algorithm was changed to operate on two low-level scans, and with the help of vertical continuity requirements, to attempt to discriminate true features from false features. In order for two features at different elevation scans to satisfy the vertical continuity requirement, it is necessary for the center of one feature to be within the "vertical continuity box" of the other feature. The "vertical continuity box" of a feature is described by a rectangle extending 5 km either side of a line connecting the

two end points of the feature, then aligning the center of this box with the center of the feature (Figure 2). The reason that the vertical continuity box extends the full length of a feature is that, while the radar may detect all of the gust front at one elevation scan, it is possible that at the other scan, only a small portion may be detected, due to either scanning above most of the gust front, or blockage by ground clutter. If this is the case, and we were to use a smaller box, it is also possible that the smaller feature would be off to one side of the larger feature, and therefore, the vertical continuity requirements would not be met. Preliminary testing shows that using two low-level scans to identify only those features having vertical continuity, results in an ~ 80% reduction in the false alarm rate over just using one low-level scan, with no loss in detection capability.

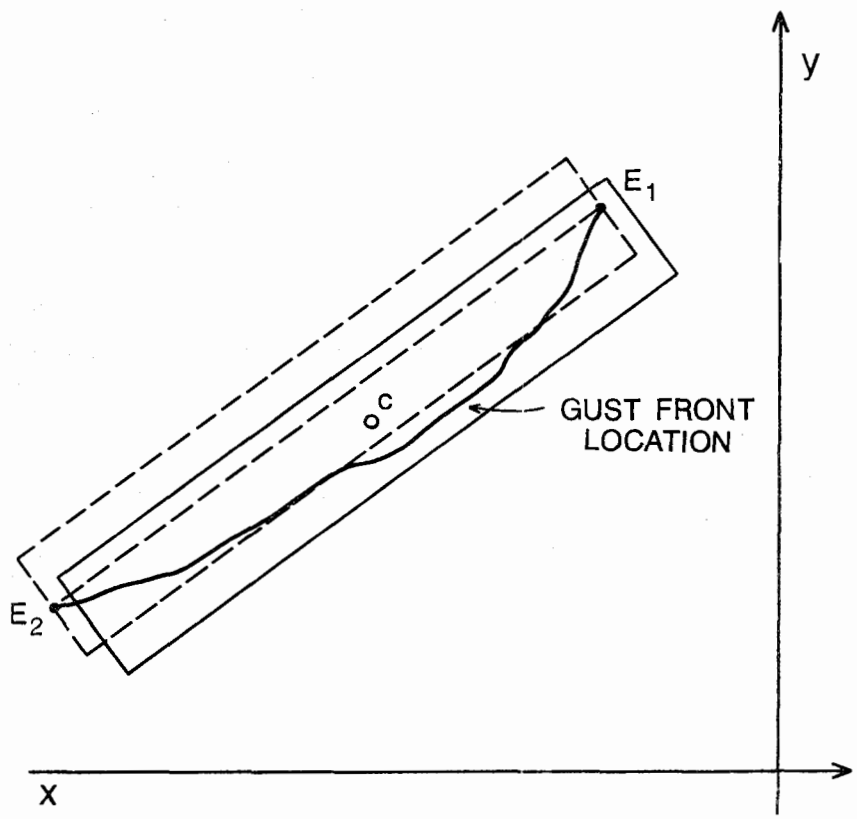

Figure 2. Geometry of the vertical continuity box. Initially determined size is dashed and the solid line box is its final location.

c. Estimates of the Wind Velocity Ahead and Behind the Gust Front

Incorporated as part of the gust front algorithm is a separate algorithm to estimate horizontal wind, ahead and behind the gust front, from radial velocities obtained by a single radar. The algorithm is a modified version of a procedure known as the Sectorized Uniform Wind (SUW), and is thoroughly discussed in the report by Smith (1986). A cursory discussion of its use in the gust front algorithm is given in the following paragraphs.

As implied by its name, the SUW algorithm relies on the assumption of uniformity of the wind, over spatial sectors, to estimate the horizontal wind. We will refer to these sectors, which are later to be specified, as data windows. Within these data windows, the assumed relationship between the horizontal wind and the radial velocity is

$$v_r = u_o \sin\theta \cos\phi + v_o \cos\theta \cos\phi \qquad (2)$$

where v_r is the radial velocity, u_o and v_o are the east-west and north-south components of the vector wind, θ is azimuth angle measured relative to north, and ϕ is radar elevation angle. For reasons made apparent by Smith (op. cit.), the mean vertical component of the wind, w_o, has been neglected in (2). The unknown quantities u_o and v_o are estimated from a matrix of radial velocity measurements, dimensioned in range and azimuth, using the method of least-squares. More precisely, the measurements of radial velocity, v_{ri}, within a data window are regressed on the spatial varying functions $(\sin\theta_i \cos\phi)$ and $(\cos\theta_i \cos\phi)$ to obtain the estimates $\hat{u}_o$, $\hat{v}_o$. It is assumed that the processed radial winds are from the lowest elevation angle of each volume scan.

We choose two data windows over which we apply (2) based on the detected position of the gust front in range and azimuth relative to the radar (see Figure 3). The detected position is the least-squares fitted curve through the points of maximum convergent radial shear, for all pattern vectors which describe the gust front (see Uyeda and Zrnic', 1986). We see that these data windows, which are located on either side of the gust front, are specified by distance from the gust front, δr, their range width Δr (same for all radials), and azimuthal width, $\Delta\theta$. All parameters may be adjustable with optimal dimensions yet to be determined. Because the magnitudes of random errors in $\hat{u}_o$, $\hat{v}_o$ are principally controlled by $\Delta\theta$ and inversely related to it,

a minimum threshold on $\Delta\theta$ keeps these estimation errors tolerable. Random errors in least-squares estimates arise because errors are made in the measurements of radial velocity. Typically, we assume all measurements have the same expected uncertainty. Then, the data window geometry determines a scaling factor which multiples this measurement uncertainty to obtain the estimate uncertainty. A further reduction in the uncertainty of wind estimates is realized when radar data are analyzed over a range interval as well (i.e., over Δr). Processing in range has the same effect as averaging. Finally, the data windows are displaced in range by an amount (δr) from the detected position of the gust front. This is to avoid "mixing" Doppler velocity data across the zone of maximum radial shear when applying the SUW algorithm. It has been found that large departures of the wind from uniformity introduce large systematic errors in the SUW estimates. An in-depth error analysis can be found in Smith (op. cit.).

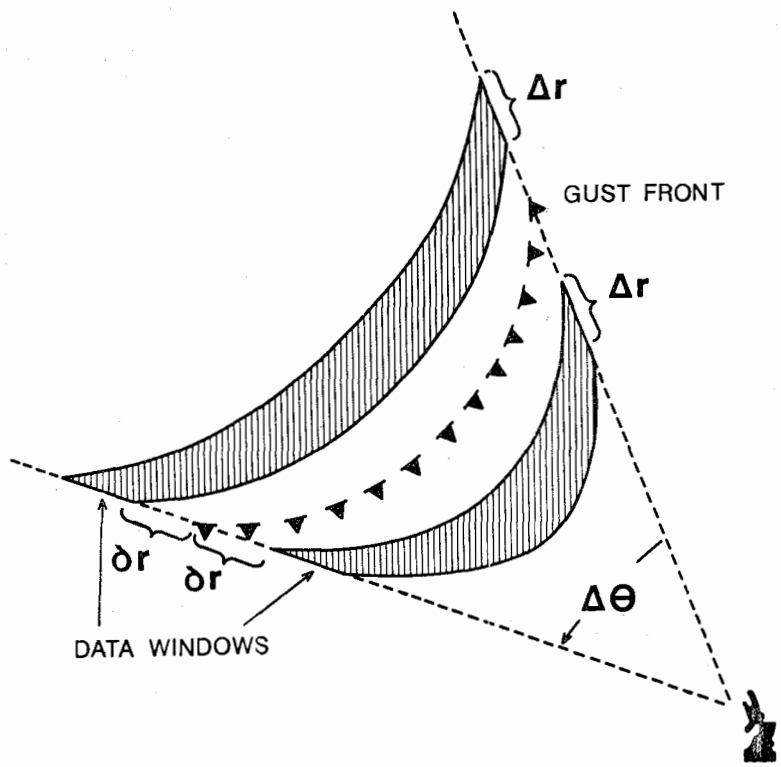

Figure 3. Schematic showing detected gust front and the two data windows over which we estimate the horizontal wind. The adjustable parameters Δr, $\Delta\theta$, and δr are identified.

The designated locations of these data windows relative to the detected gust front can best be illustrated with examples. Figure 4 shows schematics illustrating possible orientations of gust fronts relative to the radar (located in the center of the figure) and the data windows where Doppler data are processed to obtain mean wind estimates. (The present version of the gust front algorithm does not have the capability of measuring azimuthal shear and hence detecting gust fronts parallel to radar radials. Consequently, we will only concern ourselves with those gust fronts with orientations nearly perpendicular to radar radials.) For example, in Figure 4a, the center azimuth of the gust front is at a range nearer the radar than its end points. In addition, let's assume that the azimuthal width is found to be less than the minimum threshold we imposed on $\Delta\theta$. Therefore, data at an equal number of

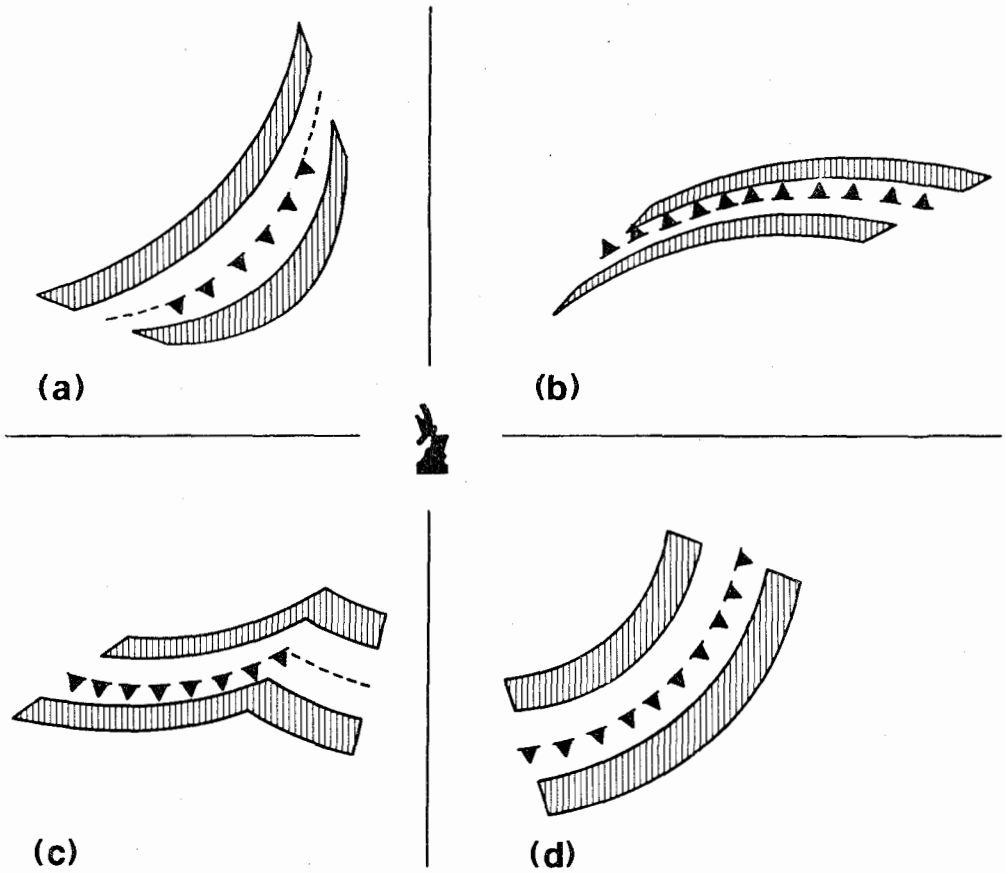

Figure 4. Illustrations of possible gust front orientations and the data windows over which we estimate the horizontal wind.

azimuths on either side of its end points are used to construct an appropriate data window (i.e., so that the azimuthal extent of the data window is at least $\Delta\theta$ wide). In Figure 4c, the azimuthal extent of the gust front is below the imposed minimum threshold and its orientation is such that the range at one end point is closer to the radar than its center range and other endpoint. In this case, the data window is extended in azimuth, at constant range, from the end point of the gust front closest to the radar. Further examples (Figures 4b and 4d) show differing orientations of gust fronts and the resulting data windows. The important point is that when the gust fronts are of azimuthal width at least equal to the minimum threshold (i.e., $\Delta\theta$), data over the entire azimuthal width of the gust front are used to estimate the mean horizontal winds; otherwise, the azimuthal width of the analysis region must be extended.

4. PRELIMINARY TEST RESULTS

a. Test Results for the Gust Front Algorithm

To be classified as a significant gust front, a radial velocity difference, Δv, of at least 5 m s^{-1} and a radial shear of at least 2 m s^{-1} km^{-1} must extend over an azimuthal length of 5 km or more, and persist at least 10 minutes. We further classify the strength of a gust front based on the average radial velocity difference over its azimuthal extent as follows: weak, Δv = 5-9 m s^{-1}; moderate, Δv = 10-14 m s^{-1}; strong, Δv = 15-25 m s^{-1}; and severe, Δv > 25 m s^{-1}. The determination of correct and false algorithm detections was based on the single Doppler radar reflectivity and velocity fields. Most false detections occurred in the ground clutter as the low-level winds and ground clutter interacted to produce false shear zones. Occasionally, a non-gust front shear zone was detected in an area of active convection (e.g., secondary surge or obstacle flow). These were considered as neutral detections, and not counted as either correct or false detections. Because the purpose of the algorithm is to detect and track only those gust fronts that are approaching or receding from the radar, gust fronts with orientations nearly parallel to the radar beam will likely not be detected, or may be classified as weaker than they actually are.

Preliminary tests were run for the latest version of the gust front algorithm on the following cases from the National Severe Storms Laboratory (NSSL), FAA/Lincoln Lab, and the National Center For Atmospheric Research

(NCAR). They are:

1) 3 NSSL cases	4/13/81, 2105-2127 CST, five volume scans
	5/9/81, 0006-0048 CST, four volume scans
	4/26/84, 2028-2052 CST, five volume scans

Data for each of these cases encompassed strong to severe gust fronts (maximum radial velocities behind the gust front were 25-30 m s^{-1}) whose lengths varied from 15 to 55 km. Using the thresholds shown in Table 1, the algorithm worked very well in detecting and tracking the gust fronts. For the 4/13/81 and 5/9/81 cases, there were no false alarms. For the 4/26/84 case, there was either zero or one false alarm per volume scan, with the average being 0.6 per volume scan. The algorithm outputs for these three cases were in agreement with the results of Uyeda and Zrnic' (1985).

2) 1 FAA/Lincoln Lab Operational Weather Study (FLOWS) case: 5/28/85, 1558-1651 CST, eleven volume scans

This case started out as a small, narrow, weak gust front (maximum radial velocities behind the gust front were 6-9 m s^{-1}). It later developed into a broader, more diffuse outflow. In order to detect this feature, it was necessary to reduce the minimum velocity difference threshold (min Δv) to 5 m s^{-1}, the peak shear threshold to 2 m s^{-1} km^{-1}, and the minimum length threshold to 3 km. Even then, detection occurred only about half of the time, due to the weak nature of this front. Surprisingly, even with this significant reduction in the thresholds, there were no false alarms. An example of algorithm output for one of the times when the gust front was strongest is shown in Figure 5.

3) 1 NCAR Classify, Locate, and Avoid Wind Shear (CLAWS) case: 7/25/84, 1621-1728 MST, fourteen volume scans

This case consisted of one long, weak to moderately strong convergence line and several small, weak to moderately strong gust fronts (maximum radial velocities behind the gust front of 6-12 m s^{-1}). Initial tests with the thresholds in Table 1 (set for the strong Oklahoma cases) resulted in the detection of about half of the convergence line during the times it attained a moderate strength; weaker portions were not detected. None of the small scale gust fronts were detected, and there were no false alarms. The thresholds for min Δv and peak shear were then reduced to 5 m s^{-1} and 2 m s^{-1} km^{-1}, respectively, duplicating two of the reduced thresholds in the FLOWS case. With

this change we were able to detect all of the convergence line and the small scale gust fronts. However, this brought about an increase in the false alarm rate to an average of one per volume scan. Figure 6 shows algorithm output for both sets of thresholds near the time of maximum shear along the convergence line.

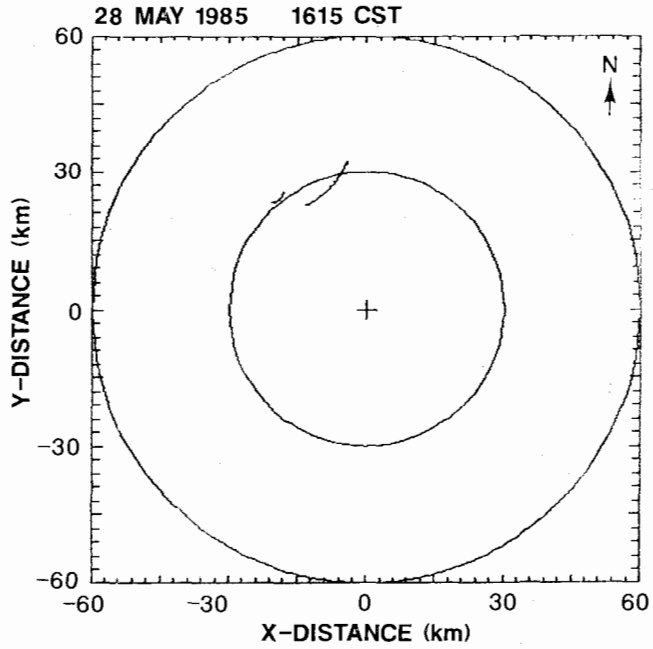

Figure 5. Algorithm output for the Memphis gust front of May 28, 1985 at 1615 CST. Range marks are at 30 km intervals.

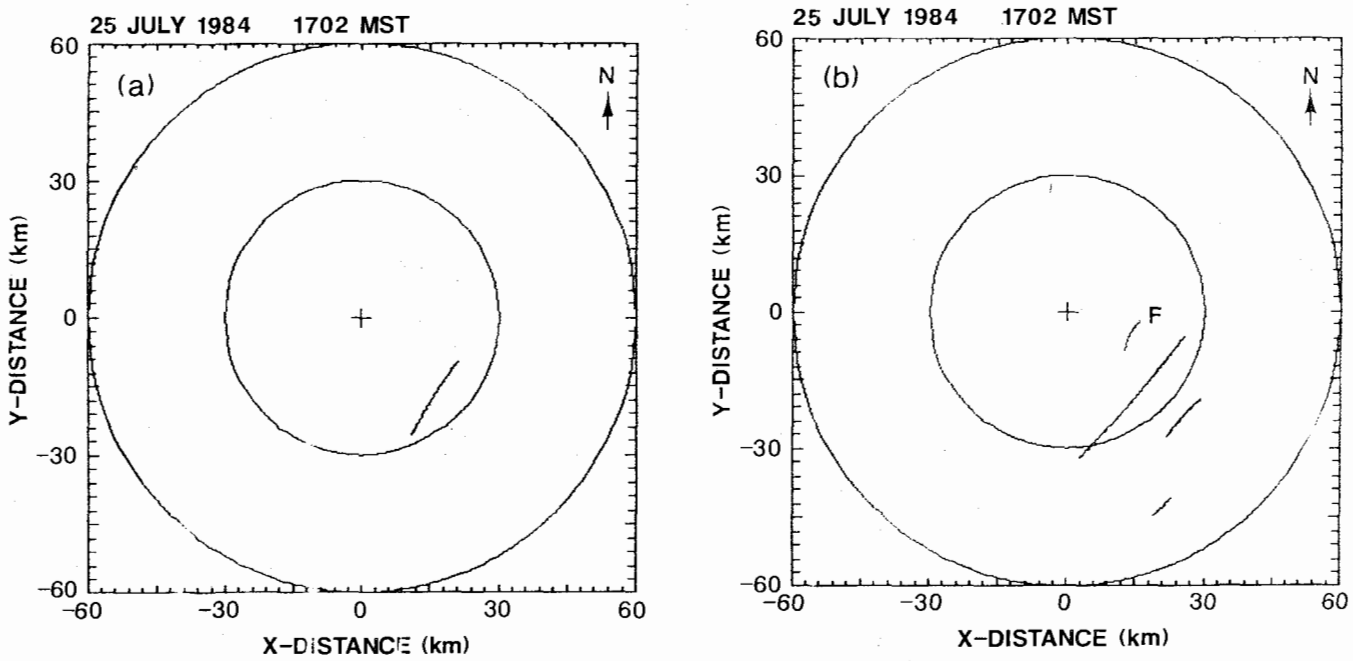

Figure 6. Algorithm output for the Denver gust front of July 25, 1984 at 1702 MST for peak shear and min Δv thresholds of a) 4 m s^{-1} km^{-1} and 10 m s^{-1}, and b) 2 m s^{-1} km^{-1} and 5 m s^{-1}. Range marks are at 30 km intervals. An "F" indicates a false feature.

Since the above results from the FLOWS and NCAR cases showed that a reduction in the thresholds, in order to detect smaller, weaker features, did not result in a large increase in false alarms, a check was made to see the effect such a reduction would have on one of the stronger Oklahoma cases. Therefore, a second test using the 4/26/84 case was run with the min Δv threshold at 5 m s^{-1} and the peak shear threshold at 2 m s^{-1} km^{-1}. This time, however, a large increase in false alarms did result, with the average increasing from 0.6 per volume scan to 3.6 per volume scan. What this seems to show is that, for the dynamically stronger weather environments associated with long, intense gust fronts, it is necessary to retain the thresholds at their original values in Table 1 to keep the false alarm rate low, whereas, for the dynamically weaker weather environments associated with smaller, less intense gust fronts, it may be possible to reduce the thresholds and still have a low false alarm rate. Figure 7 shows algorithm output for both sets of thresholds at 2037 CST.

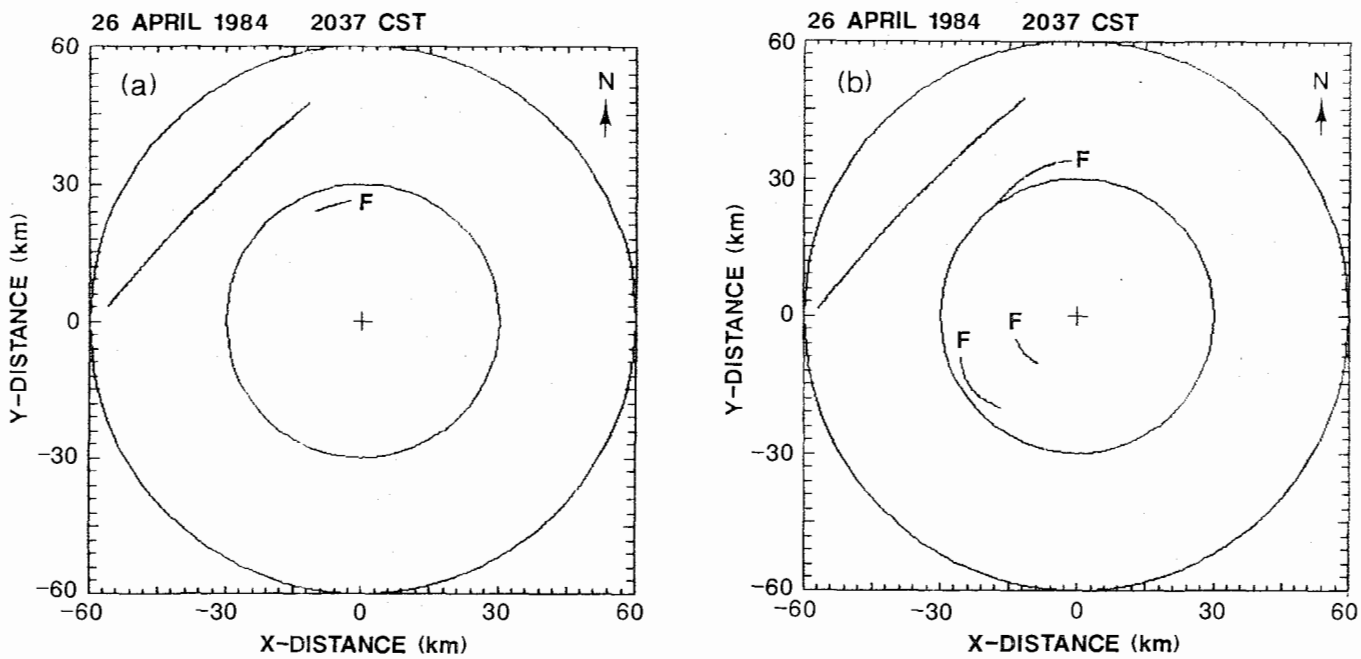

Figure 7. Same as Figure 6, except for the Oklahoma gust front of April 26, 1984 at 2037 CST.

What the above results show is that the performance of the gust front algorithm depends largely on what type of feature it is to detect, which in turn determines the values of the thresholds to be used. With the original thresholds, the algorithm works very well at detecting the larger scale, strong gust fronts associated with fast-moving squall lines and bow echoes; false alarms are few, if any. As the thresholds are reduced to detect weak to moderate gust fronts, the number of false alarms generally goes up. Therefore, a decision must be made as to what the proper balance should be between trying to detect increasingly weaker gust fronts with a corresponding potential increase in the false alarm rate, bearing in mind that lowering the thresholds in the more dynamic weather situations is much more deleterious to the false alarm rate than similar reductions of the thresholds in less dynamic weather conditions.

b. Test Results for the Sectorized Uniform Wind Algorithm

Three gust front cases in central Oklahoma were chosen to test the SUW algorithm; April 13, 1981, May 9, 1981, and April 26, 1984. These, as well as some other cases, are documented in detail in the report by Uyeda and Zrnic' (1985). Doppler velocity displays for several of the analysis times can be found in the above cited report.

We compared the wind output from the SUW algorithm with other supplemental wind data such as that available from Stationary Automated Mesonetwork (SAM) sites. When available, winds from rawinsonde and those measured by an instrumented tower were used to judge SUW results. Comparisons of rawinsonde data with SUW estimates are best made ahead of the gust front since both these measurements represent to some extent the ambient environmental wind. Furthermore, the wind ahead of the front tends to be fairly uniform and thus complies with the basic assumption of the SUW algorithm.

For these three analyzed cases, the following values for the parameters describing the data window size and location were used: $\Delta\theta = 40°$, Δr ranged between 2.25 km and 3.15 km, and δr ranged between 450 m and 630 m, depending on the radar setup. The radial spacing of the velocity data was either 150 m corresponding to the first set of values for Δr and δr, or 210 m corresponding to the second set of values.

April 13, 1981:

Figures 8a and 8b illustrate the wind comparisons made at 2111 CST and 2123 CST, respectively. At approximately 2120 CST, a rawinsonde was released from Tuttle, Oklahoma (TTS). TTS is located almost due west of the NSSL radar (NRO) near 36 km range. The rawinsonde winds up to 1 km above ground level (AGL) are shown on Figure 8b. Mesonetwork wind data recorded at analysis time are superimposed on the figures.

At 2111 CST, general agreement between SUW estimated wind direction and those of the mesonetwork data is apparent (Figure 8a). On the other hand, the wind speeds for the SUW estimates tend to be higher. This is most evident ahead (east) of the gust front. However, the radar data used to compute the SUW estimates are from near 750 m AGL, whereas the mesonetwork data are representative of winds near the ground. Furthermore, examination of Doppler displays indicate radial velocities near 11 m s^{-1} immediately ahead of the gust front and near 19 m s^{-1} immediately behind. Thus the SUW estimates of wind magnitude agree reasonably well with the largest measured radial winds.

At 2123 CST (Figure 8b), considerable differences are observed not only between SUW estimated winds and the SAM winds but also between the SAM winds and those measured from the rawinsonde. For example, the surface measurement at the rawinsonde site differs nearly 10 m s^{-1} in wind speed from a SAM measurement, even though this network station is located only a few kilometers to its north. In general, however, the network stations consistently indicate weak, westerly winds in advance of the gust front, which veer to the northwest behind the gust front with speeds near 15 m s^{-1}.

From inspection of the Doppler velocity display at this same time (see Figure 13 in Uyeda and Zrnic', 1985) we conclude that the SUW estimate of wind direction ahead of the front is reasonable. It not only agrees well with the rawinsonde winds at the same altitude (radar beam height about 400 m AGL), but the line of zero Doppler velocity is aligned nearly perpendicular to the estimated wind direction. From the magnitudes of the Doppler winds ahead of the front, we can not easily assess the accuracy of the estimated wind magnitude but we note general consistency between the two; the Doppler winds are relatively weak (magnitudes less than 10 m s^{-1}) and so is the SUW wind. Behind the front, mean wind direction is difficult to determine because of the diverging nature of the outflow. However, velocity aliasing has occurred, in-

dicating winds in excess of 23 m s^{-1}, which is again consistent with the SUW wind of 24 m s^{-1}.

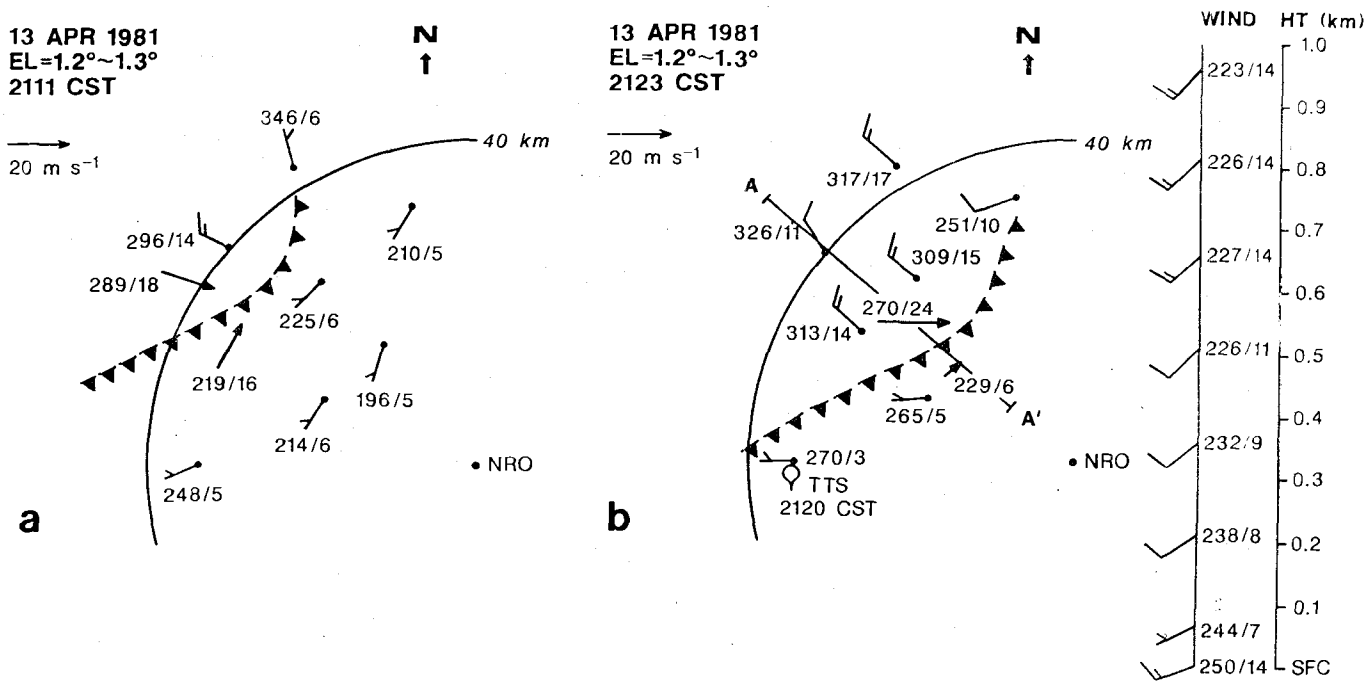

Figure 8. April 13, 1981 Oklahoma gust front case showing detected position at a) 2111 CST and b) 2123 CST. SUW estimates are denoted by arrows with arrow length proportional to wind speed and arrow orientation indicating wind direction. Mesonetwork wind data are plotted as barbs with flags next to their numerical values. Long flags indicate 10 m s^{-1}, short flags indicate 5 m s^{-1}. The 2120 CST TTS rawinsonde winds up to 1 km AGL are shown in (b). The rawinsonde launch site is indicated with a balloon. The line labeled AA' describes the location of the horizontal cross-section shown in Figure 9.

Figure 9 illustrates a horizontal cross-section through the gust front at 2123 CST showing reflectivity factor and radial velocity along the 310° radial. Radar beam elevation angle is 1.2°. The detected position of the gust front (G), and the beginning (B) and ending (E) range of the pattern vector are indicated. The range limits of the two data windows are also shown. As illustated, the region outlined as the pattern vector is characterized by convergent radial shear.

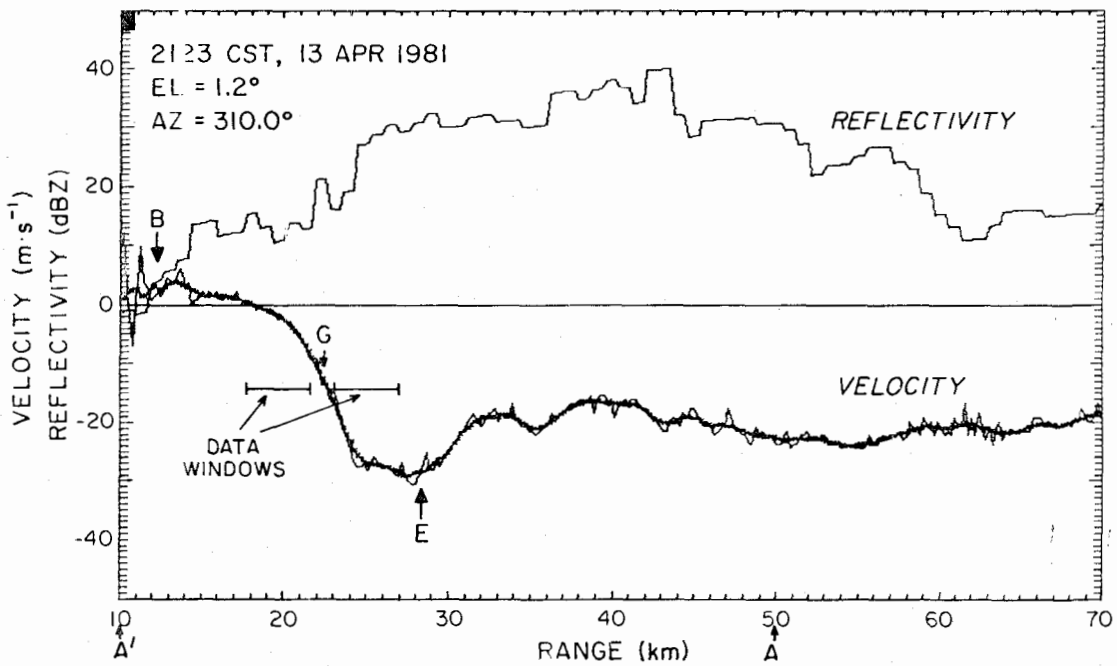

Figure 9. Horizontal cross-section along line AA' shown in Figure 8b. Reflectivity factor Z (dBZ), radial velocity (m s^{-1}), and a nine-point average mean velocity are given. "B" and "E" denote the beginning and ending range of the pattern vector. "G" is the detected position of the gust front. The location and length, in range, of each data window is shown.

An observed characteristic of many thunderstorm outflows is a wind maximum immediately behind the gust front [Figures 12 and 13 in Eilts (1986a) are good examples]. Goff (1976) attributes this to a solenoidal circulation near the boundary between cold outflow and warm inflow, which accelerates the flow in the cold air immediately behind the gust front. In Figure 9, these peak inbound winds occur where the radial shear is zero, some 5-7 km behind the gust front. Behind this wind maximum, there is a region of moderate divergent radial shear, beyond which the winds remain fairly steady but still relatively strong. As illustrated, the data window behind the gust front encompasses, for the most part, this region of maximum winds. Therefore, it is not surprising that the SAM winds, measured well behind the gust front, are weaker in magnitude. Furthermore, as pointed out earlier, the SUW estimate represents the winds near 400 m AGL. Eilts (1986b) observed that measured outflow winds at heights above 200 m tend to be, on the average, 1.6 times larger than winds measured at the surface. If we multiply the surface wind speeds by a factor of 1.6, they agree quite well with the speeds measured aloft.

May 9, 1981:

Figures 10a and 10b illustrate the SUW output for 0018 and 0032 CST, respectively. Very little supplemental wind information is available, primarily due to the far range of the gust front (i.e., it is outside the range of the surface mesonetwork). In addition, there was no proximity rawinsonde release. Therefore, much of our assessment of the accuracy of the SUW estimates relies on inferences drawn from the Doppler velocity displays.

At the earlier time (0018 CST), SUW output indicates a pronounced wind shift across the front of nearly 90° (195°/13 m s^{-1} to 282°/17 m s^{-1}). Unfortunately, all available surface observations occur well to the east. We did find, however, that the line of zero Doppler velocity ahead of the front agrees quite well with the SUW estimate of wind direction. Fortunately, by 0032 CST, the gust front position was near the western edge of the SAM network. At this later time, the SUW estimate ahead of the gust front compares extremely well with the surface observations both in speed and direction. There is no surface wind information available for comparison behind the gust front. The 0033 CST Doppler velocity display (see Figure 21 in Uyeda and Zrnic', 1985) indicates near 20 m s^{-1} radial winds immediately behind the gust

front. The strength of these winds are in close agreement with the horizontal wind estimated from the radial velocity measurements.

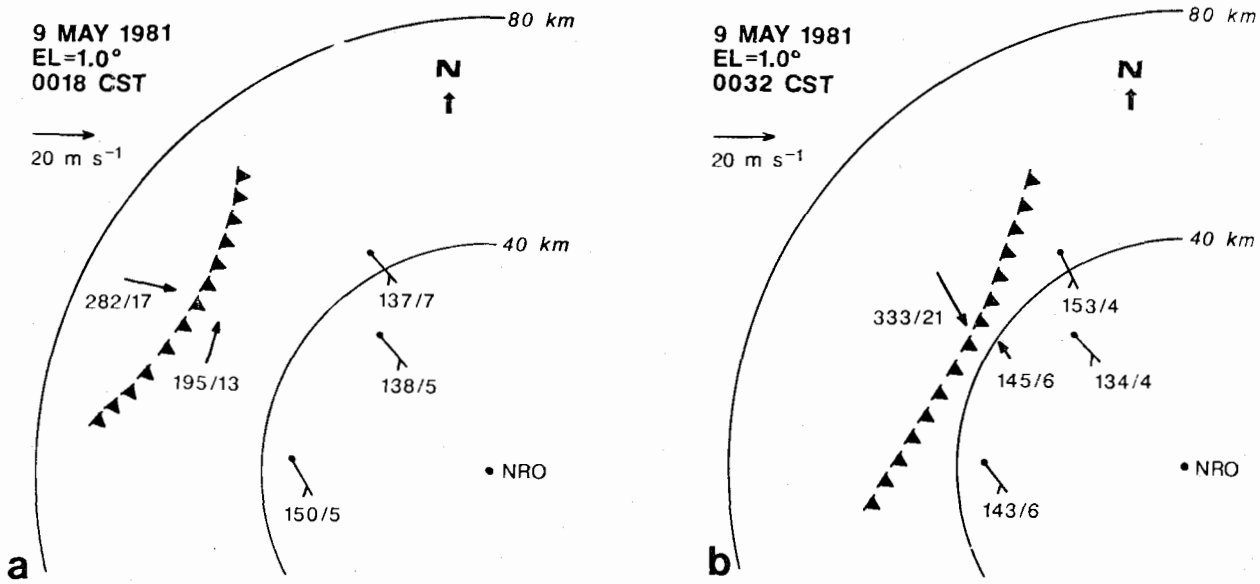

Figure 10. May 9, 1981 Oklahoma gust front case showing detected position at a) 0018 CST and b) 0032 CST. Symbols are as defined in Figure 8.

April 26, 1984:

Like the April 13, 1981, gust front case, there is an abundance of supplemental wind data on this day. Figures 11a and 11b illustrate the wind comparisons for 2042 and 2052 CST, respectively. A rawinsonde release from CHK (Chickasha, Oklahoma) occurred at 2047 CST. The CHK launch site is located approximately 40 km southwest of Norman (NRO). The rawinsonde wind data is plotted in Figure 11b for the lowest kilometer.

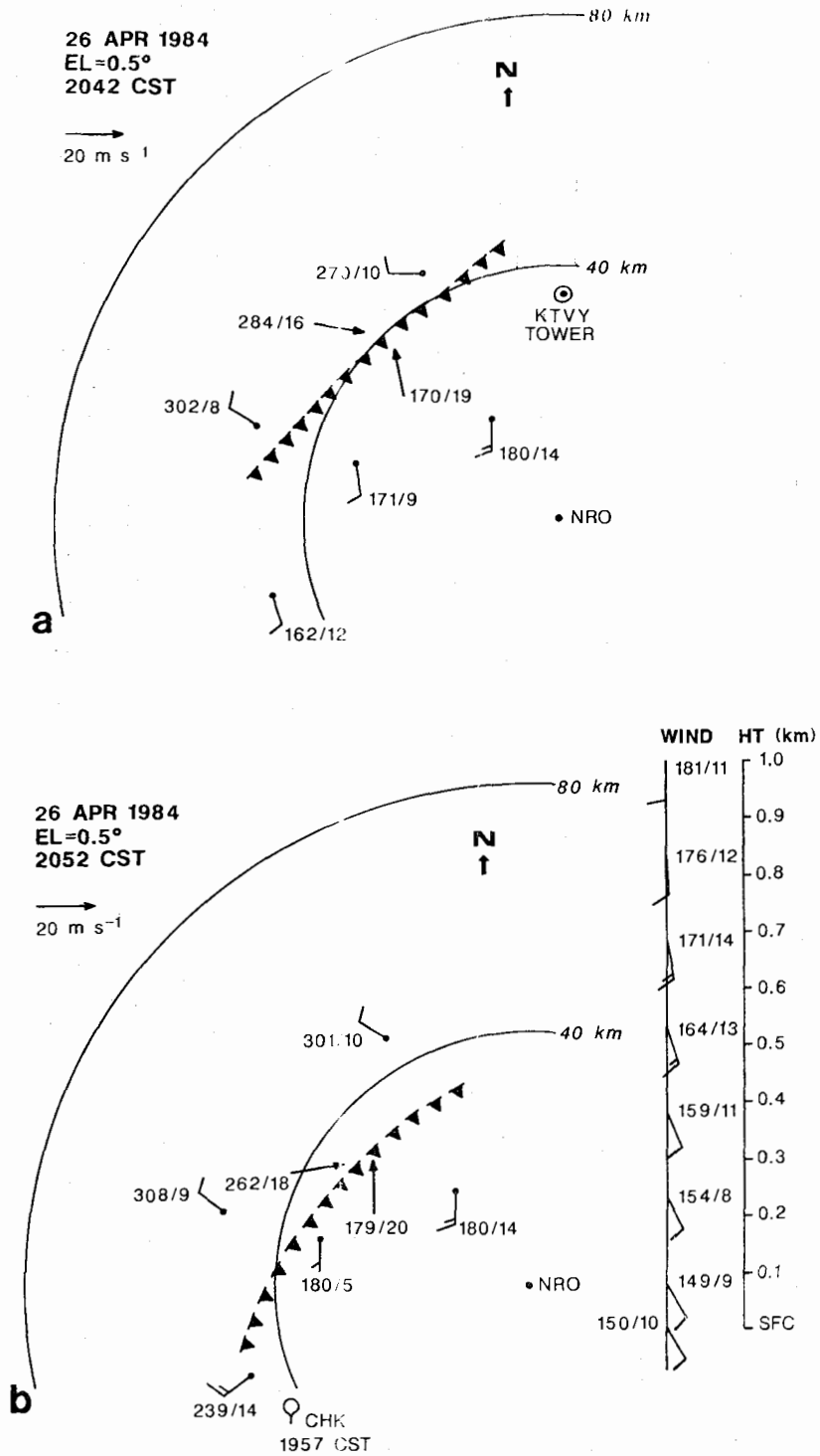

Figure 11. April 26, 1984 Oklahoma gust front case showing detected position at a) 2042 CST and b) 2052 CST. Symbols are as defined in Figure 8. The 1957 CST CHK rawinsonde winds up to 1 km AGL are shown in (b).

At 2042 CST, the leading edge of the gust front is located around 40 km northwest of NRO, well within the SAM network. We see excellent agreement between the SUW estimated wind directions and those measured at the surface. Again the magnitudes of the SUW estimates are slightly larger. The line of zero Doppler velocity on the 2037 CST display indicates south-southwest winds ahead of the gust front, which is in excellent agreement with the SUW estimate of direction.

Comparisons made at 2052 CST (Figure 11b) show generally small differences. The SUW estimate ahead of the front indicates a relatively strong, southerly wind (20 m s^{-1} at 179°). The rawinsonde measured winds near the same height (approximately 300 m AGL) are more southeasterly and much weaker (10 m s^{-1} less), which is expected because the SUW estimates are derived from radar data very near to the front where accelerations of the environmental flow occur. Behind the gust front, the SUW estimate indicates a westerly wind of 18 m s^{-1}, whereas the surface values are more northwesterly and quite a bit weaker.

In addition to the rawinsonde, there were wind measurements from the instrumented KTVY-TV tower located in Oklahoma City, some 36 km north of Norman. The tower is instrumented at seven heights, the highest level is at 444 m AGL. One minute averages of wind speed and direction at the seven recording levels are shown in Table 2 for 2042 CST (several minutes prior to gust front passage) and 2100 CST (approximately 4 minutes after the gust front passed the tower).

The wind speeds recorded at the tower, above 177 m and prior to gust front passage, are in better agreement with the prefrontal wind speeds estimated from the Doppler radial winds than those measured by the rawinsonde near the same heights (see Fig. 11a and b). Furthermore, the wind directions match the SUW estimates extemely well. Following gust front passage of the tower, around 2100 CST, an overall westerly wind is indicated, which is in better agreement with the SUW estimates of wind direction than those from SAM measurements. This is not surprising since the tower recorded winds at 226 m and 444 m are near the heights represented by the radar data used in the SUW analysis. What is somewhat surprising is that the SUW estimates of wind speed overestimate, by 50%, the wind speeds measured at the upper levels of the tower. This might well be explained by the fact that the tower is located a

minimum of 20 km from the centroid of the gust front where the SUW estimates are most representative. We believe that the SUW estimates are reasonable because the Doppler velocity fields, at the times of the SUW analyses, indicate winds behind the gust front much stronger than the tower winds recorded at 2100 CST.

Table 2. Tower Data at 2042 and 2100 CST for the April 26, 1984 Gust Front Case.

Time	2042 CST	2100 CST
Level	Direction (°)/Speed (m s^{-1})	Direction (°)/Speed (m s^{-1})
SFC	168/13.9	274/11.1
26 m	170/15.6	278/11.3
45 m	175/15.9	278/12.0
89 m	171/15.9	276/12.3
177 m	169/19.3	274/13.4
266 m	171/23.7	272/12.8
444 m	170/27.0	244/10.0

c. Comparison of SUW Estimates With the Propagation Speed of the Gust Front

The propagation speed of the gust front can readily be determined if its position is known at two consecutive times, t_1 and t_2. Because parts of the gust front may move relative to each other, thus causing a change in shape, a mean speed is calculated over some time interval $\Delta t = t_2 - t_1$ from the displacement of its centroid. The centroid is defined by the gust front's center range and azimuth (Eqs. 5 and 6 in Uyeda and Zrnic', 1985).

The three analyzed cases present opportunities to compare the propagation speed with the SUW estimates of wind. Various relationships between the propagation speed of the gust front and the mean wind components ahead and behind the gust front, and normal to the frontal boundary, have been proposed.

Goff (1976) suggests that the winds in the warm air (i.e., ahead of the gust front) have little influence and that the propagation speed can be described quite accurately as two-thirds of the peak wind measured behind the gust front. In Table 3, we list the estimated propagation speed along with the SUW estimates of wind behind the front.

Table 3. Gust Front Propagation Speeds Obtained From Two Consecutive (In Time) Centroid Positions Along With SUW Estimates of the Wind Behind the Gust Front for the Earlier of the Two Times.

DATE	CENTROID TRACKING		SUW ESTIMATE BEHIND GUST FRONT	
	DIRECTION (°)	SPEED (m s^{-1})	DIRECTION (°)	SPEED (m s^{-1})
4/13/81	288	18	289	18
5/09/31	303	19	282	17
4/26/84	28	12	284	16

For the two cases in 1981, the SUW estimated winds and the propagation speeds agree reasonably well, i.e., no scaling factors are required to match the SUW estimate with the speeds determined from centroid tracking. A large discrepancy exists for the 1984 case, however. Although the displacement of the centroid indicates a movement to the south-southwest, Figures 8a and 8b clearly show movement to the southeast. We believe, in this case, that the SUW estimate of wind agrees better with the actual propagation speed than that obtained from centroid tracking. A problem that plagues the tracking of larger gust fronts, such as the one on 4/26/84, is that the centroid position can change dramatically in the direction along the front, for relatively small changes in gust front position. Furthermore, if at some time part of the gust front becomes aligned along radar radials, propagation speeds obtained from tracking centroid positions may be totally unrepresentative of the true propagation speed. More reliable estimates of propagation speed might be obtained if relationships such as those found by Goff (1976) are used.

d. General Comments on the SUW Algorithm

One of the objectives of incorporating the SUW algorithm into the gust front algorithm is to estimate the wind shear across the front. As is well known, this is invaluable information to pilots because it quantifies the hazard and thus aids in aircraft safety. Surface-based sensors can always provide wind information near airport runways. However, Doppler radar can supply the winds some distance from the airport, possibly well in advance of gust front passage. This wind information can aid air traffic controllers in decision making for changing runways. With the three cases presented, a sample of the performance of the SUW algorithm was given. Quantitative comparisons were limited by the availability of wind data from the SAM network, rawinsondes, and the tower.

It is important to consider situations which, when they arise, may make it difficult to estimate the horizontal winds from single Doppler radar measurements. As is well known, the minimum height at which the gust front can be detected by radar depends on several factors, many of which the radar operator has little or no control over. For instance, the earth's curvature sets a lower limit to the observation height at any range. At near ranges, the earth's curvature may not be of great concern. However, the gust front can become "lost" in the ground clutter. Ground clutter cancellors should alleviate this problem somewhat and allow tracking very near the radar site. It is at these close ranges that the accuracy of SUW estimates degenerates if tracking is accomplished by increasing the elevation angles of observation. Smith (op. cit.) shows that random errors in wind estimates are inversely related to $\cos^2\phi$. In addition, artifacts such as range overlaid echoes and velocity aliasing need to be considered. Velocity aliasing may make SUW estimates useless.

Furthermore, we need to consider the parameters which describe the data window and its position relative to the detected gust front. Although we used 40° as the minimum threshold for $\Delta\theta$, we can tolerate azimuthal widths as small as 30°. Random errors in SUW estimates do not increase substantially for this smaller value. One advantage of processing Doppler data over smaller sectors is that more reliable estimates of the winds behind the smaller gust fronts may be possible, particularly for those gust fronts which are of azimuthal width less than the minimum threshold imposed on $\Delta\theta$. This is because less data "outside" the bounds of the gust front would be used. In addition, the

effects of nonuniformities of the wind on SUW estimates tend to be less over these smaller sectors (see Smith, op. cit.).

Although the range width Δr was chosen arbitrarily, we need to place an upper limit on this value as well. As the elevation angle increases, the radar beam traverses an increasing increment in height for a given range interval. Conversely, for a given elevation angle, increasing the range interval increases the height increment. This may present problems if vertical wind shear is large. Vertical shear, as well as other nonuniformities such as secondary surges and downdrafts, contaminate SUW estimates. Therefore, the range widths must not be excessive; otherwise, the basic assumption of a uniform wind over the analysis area are likely to be violated. We believe range widths less than 10 km are acceptable.

Finally, the range displacement of the data windows from the detected range of the gust front δr may need to be adjusted. As discussed earlier, the strongest winds are displaced somewhat behind the gust front. Presently, the data window behind the gust front encompasses, for the most part, the strongest winds. It may be necessary to use two data windows so that we not only estimate the strongest winds, but also the more sustained winds well within the thunderstorm outflow. The data window ahead of the gust front may need to be further displaced so that it is situated some distance away from the updraft region, which generally occurs in the warm air as it is lifted over the cold outflow. Goff (op. cit.) has found this updraft region to be narrowest in the horizontal direction near the surface, typically no more than a kilometer wide; the updraft region then broadens with height to, at most, several kilometers. Displacement of the data window by at least 5 km would assure that the estimated winds are not influenced by the pre-frontal updraft.

5. VERIFICATION OF GUST FRONT ALGORITHM OUTPUT

a. Comparison of the Gust Front Position with Surface Stations

To determine how well the location of the gust front, as indicated by the algorithm, compared with its location as indicated by surface stations, algorithm output for the three NSSL cases was compared with the surface wind direction obtained from several NSSL surface stations. Since it is not possible to determine the exact location of a gust front from a group of scattered surface stations, we decided to compare the time of passage of the wind-shift

line over the available surface sites. This was done by either interpolating or extrapolating, in time and space, the location of a detected gust front such that it coincided with the location of a particular surface site. A comparison was then made between this algorithm indicated time of passage and the actual time of passage as indicated by the change in wind direction at the surface site. The results are as follows:

May 9, 1981 case (Figure 12)

The gust front algorithm was run for three times: 0006, 0018, and 0032 CST. Unfortunately, no surface stations had the gust front pass over them from 0006 through 0032 CST. Therefore, in order to do a comparison, the position of the gust front was linearly extrapolated ahead in space and time to the nearest three stations. The results are:

Station number	Actual time of gust front passage (CST)	Extrapolated time of gust front passage (CST)
1	0035	0038
2	0043	0044
3	0043	0042

The extrapolation was based on the average speed of the gust front from 0006 to 0032 CST. The wind shift at all three stations was swift, with the wind direction going from SE to NW in one minute (the lowest time scale resolution for NSSL surface stations is one minute).

April 26, 1984 case (Figure 13)

The algorithm was run for three times: 2037, 2042, and 2047 CST. For this case, two surface stations are located along the detected position of the gust front at 2037 CST. The time of passage at both stations was around 2035 CST. The time of passage for this case could not be estimated as precisely as in the previous case because at both stations it took about four minutes for the wind direction to shift from S to WNW.

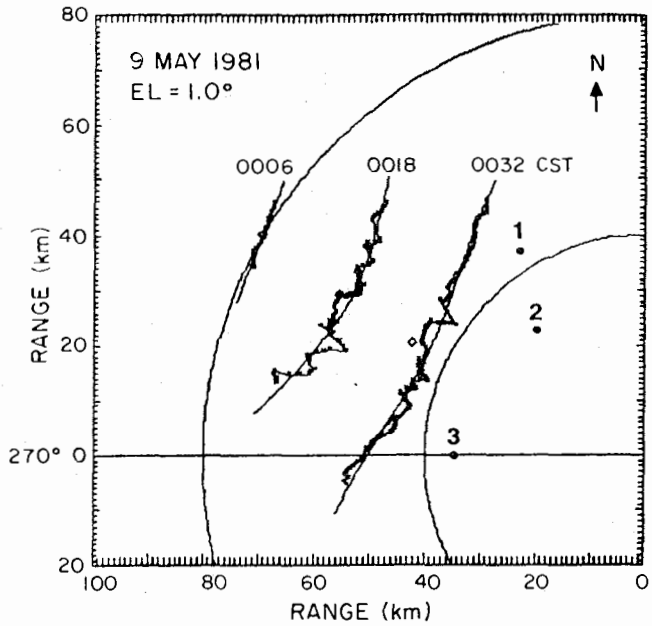

Figure 12. Plot of the algorithm output for the Oklahoma gust front of May 9, 1981 along with the locations (1,2,3) of the NSSL surface stations used for a time of passage comparison.

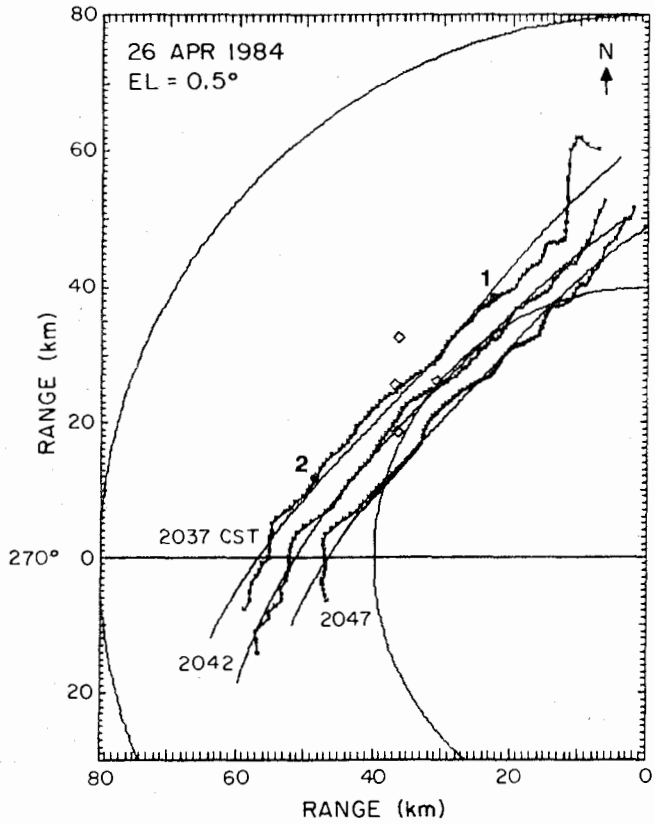

Figure 13. Same as Figure 12, except for April 26, 1984.

April 13, 1981 case (Figure 14)

The algorithm was again run for three times: 2111, 2116, and 2123 CST. Three surface stations (No. 1-3) are located on or very near to the detected gust front positions. In this case, as in the 4/26/84 case, the surface winds shifted gradually from a SSE direction to a SW direction, and finally to a NW

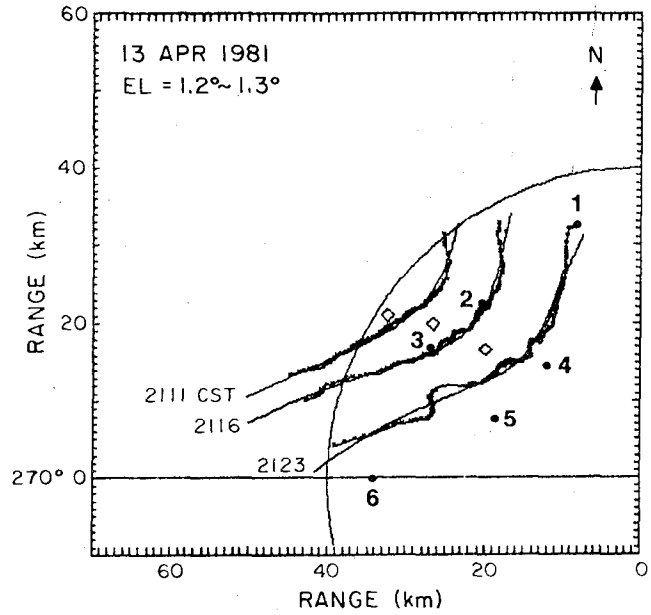

Figure 14. Same as Figure 12, except for April 13, 1981.

direction. If we use the time when the wind direction shifted past 270° for comparison, we get time differences of +1, +1, and -2 minutes for the three stations, respectively, with a positive difference meaning the algorithm indicated time of passage was ahead of the surface station indicated time of passage. For three additional sites (No. 4-6), we can extrapolate ahead in space and time the position of the gust front, as was done for the 5/9/81 case. For these three sites, the time differences are -1, -4, and -5 minutes, respectively.

What these results show is that, in most cases, there was fairly good agreement between the algorithm output and the surface stations, with the time difference being $\leq$ 5 minutes for all comparisons, and $\leq$ 2 minutes for 73% of the comparisons.

b. Comparison with a Second Doppler Radar

A second comparison of algorithm output was done by comparing the overlapping locations of gust fronts as determined from two different Doppler radars (the NSSL radars located at Norman and Cimarron (CIM), which is about 40 km NW of Norman) looking at the same gust front. The comparison was made for eight different elevation scans on 4/13/81, with the gust front located between 10 and 30 km away from each radar for the times considered. The results are given in Table 4. (There are two entries at 2127 CST and 0.4° becasue of a gap in the gust fronts detected position, as seen by the Normar radar, due to ground clutter.) The root mean squared (RMS) distance errors were calculated by using the shortest distance between any two points of the estimated gust front locations. We see that the average RMS distance error is less than 1 km, which indicates good position agreement. Figure 15 shows the algorithm output for each radar at 2127 CST for approximately the same elevation angle. From Table 4 we see that the position correlation for this particular comparison was very good, with an RMS distance error of only 0.5 km.

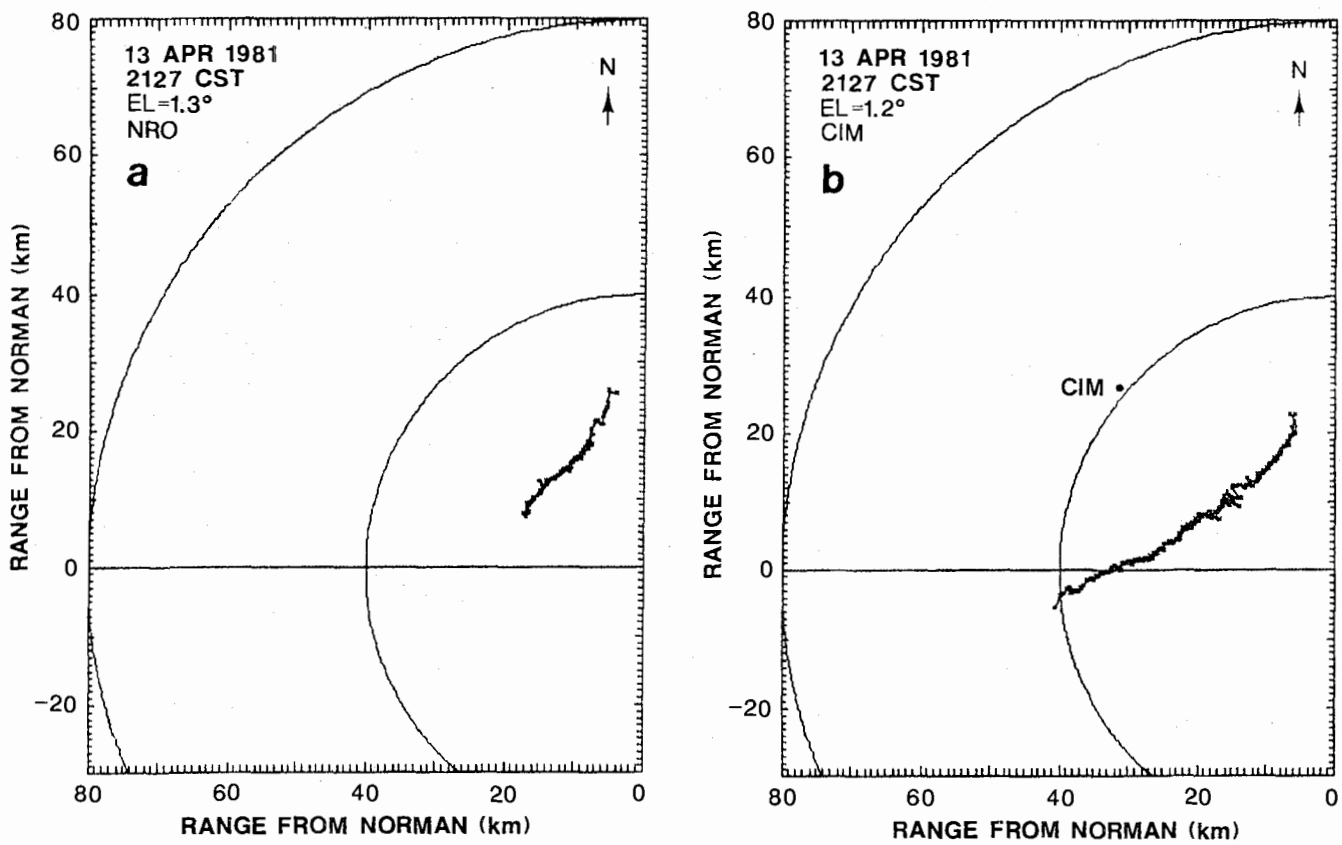

Figure 15. Algorithm output for two different radars; a) Norman (NRO) and b) Cimarron (CIM), looking at the same gust front (April 13, 1981).

Table 4

Results of the Gust Front Position Comparison for the Norman and Cimarron Radars.

Time (CST)	Elevation Angle	RMS distance error (km)	No. of points
2116	0.8°	1.4	18
2116	1.3°	1.1	23
2123	0.4°	0.7	15
2123	0.9°	0.6	27
2123	1.3°	0.7	31
2127	0.4°	1.4	28
2127	0.4°	0.5	12
2127	0.9°	0.8	76
2127	1.3°	0.5	72
	Average =	0.88	33.6

6. SUMMARY

The gust front algorithm originally proposed by Uyeda and Zrnic' (1985) was fully automated and made ready for real-time operational testing. Several changes have been incorporated in order to simplify the algorithm, and speed up its running time. Of substantial impact to operational users is our finding that it may be necessary to operate the algorithm with more than one set of thresholds. For instance, we have determined that higher shear (4 m s^{-1} km^{-1}) and velocity difference (10 m s^{-1}) thresholds are needed for strongly-dynamic weather environments, whereas lower thresholds (2 m s^{-1} km^{-1}, 5 m s^{-1}) are more suited for dynamically weaker conditions. All three Oklahoma gust fronts on which the algorithm was tested belonged to the former category, whereas one case from Denver and one from Memphis were associated with weaker weather conditions. When appropriate thresholds were used, there were very few false alarms (on average less than one per volume scan). But when lower thresholds were tried for one of the Oklahoma cases, the false alarm rate increased substantially (to about four per volume scan). Most of these were due to problems with ground clutter.

Other changes to the algorithm involved: 1) the inclusion of a routine for fitting a second-order polynomial to the gust front vector positions in cartesian coordinates, 2) inclusion of an automated vertical continuity check

using data from two low-level elevation scans, and 3) inclusion of a sectorized uniform wind procedure to determine winds ahead and behind the front.

The outputs of the algorithm were checked for consistency and compared to data from other sources. For instance, vector winds from the uniform wind analysis were compared with surface and rawinsonde observations, as well as with general trends of the Doppler velocities. Agreement was beyond our expectations; moreover, the uniform wind analysis proved, on at least one occasion, to be a better indicator of gust front motion than tracking of the centroid. Times of gust front passage over surface stations were generally within two minutes of interpolated or extrapolated positions by the algorithm. Also, in the only intercomparison between the positions obtained from two spaced Doppler radars, the average RMS errors were less than 0.9 km. We emphasize here that these good comparisons are for strong, single, well-defined gust fronts. It remains to be determined if these impressive results will be repeated in situations where multiple, weak gust fronts are present.

REFERENCES

Eilts, M.D., 1986a: "Low Altitude Wind Shear Detection with Doppler Radar", J. Climate Appl. Meteor., **25**, 96-106.

Eilts, M.D., 1986b: "Doppler Radar Measurement of Low-Altitude Wind Shear in Oklahoma", Proceedings 23rd Conference on Radar Meteorology and Conference on Cloud Physics, Snowmass, Colo., American Meteor. Soc., Boston, Vol. 3, 89-92.

Goff, R.C., 1976: "Vertical Structure of Thunderstorm Outflows", Monthly Wea. Review, **104**, 1429-1440.

Smith, S.D., 1986: "Sectorized Uniform Wind Algorithms", NEXRAD Joint Systems Program Office Report, Sept., 1986, 25 pp.

Uyeda, H. and D.S. Zrnic', 1985: "Automatic detection of gust fronts", FAA Report No. DOT/FAA/PM-85/11. Available from NTIS.

Uyeda, H. and D.S. Zrnic', 1986: "Automatic detection of gust fronts", J. Atmos. Oceanic Technol., **3**, 36-50.